



# Sensitivity Analysis of Gold Nanorod Biosensors for Single Molecule Detection

Zunaid Omair<sup>1</sup> · Muhammad Anisuzzaman Talukder<sup>2,3</sup>

Received: 18 October 2018 / Accepted: 9 April 2019  
© Springer Science+Business Media, LLC, part of Springer Nature 2019

## Abstract

Single protein molecule detection is important for investigating molecular behavior and diagnosing diseases at an early stage. Gold nanorod (GNR) biosensors have shown promise for label-free detection of single protein molecules. However, for widespread applications of GNR biosensors with high sensitivity, detail studies are needed to understand the effects of the sensing environment and the molecular binding dynamics on the sensitivity. In this work, a comprehensive theoretical analysis with variable substrate, buffer, ligand, and binding position of the target molecules shows that GNR biosensors are highly sensitive for single molecule detection of biological samples including critical pathogens such as cancer marker thyroglobulin and human immunodeficiency virus (HIV) marker glycoprotein. We also propose and show that a GNR biosensor with a dielectric cladding layer on the body increases the sensitivity by orders of magnitude compared to other state-of-the-art biosensors.

**Keywords** Plasmonic nanobiosensor · Single molecule detection · LSPR · SPP · Biosensor · Optical sensor · Photonic sensor · Optical sensing · LSPR sensor

## Introduction

The early detection of diseases, especially the diseases that have no available cure, is of critical importance. The spread of ebola and human immunodeficiency virus (HIV) can be effectively controlled with an early detection of as small as only 25% of patients [1, 2]. Similarly, early-stage detection can lead to control, and in some cases, elimination of cancer [3]. However, the challenge is to detect the presence of pathogens at the smallest possible concentration. The

necessity to detect an ultra-small quantity of a pathogen often leads to a single molecule detection, which is the ultimate precision desired. [4, 5].

Single biomolecules can be detected with and without the addition of a label. However, the label-free method is preferable as it does not require the additional processing and material costs of label-assisted methods, and also as the biomolecules are detected at their natural states. Notable label-free biosensors include field-effect transistor (FET) biosensors [6], magnetic biosensors [7], and optical biosensors [8]. While it is challenging for FET biosensors to operate at the noise level required for single molecule detection, magnetic biosensors are not quite suitable for single molecule detection due to the large detection volume that they operate on. By contrast, label-free optical biosensors show promise for their high sensitivity and low background noise. Optical biosensors based on photonic and hybrid photonic–plasmonic cavities have been used to detect single molecules by measuring the shift of resonance wavelength of whispering gallery modes [8–11]. However, these biosensors are relatively large and their sensitivity is only in the range of picometer to femtometer. Recently, localized surface plasmon resonance (LSPR) shift of gold nanoparticles has been used to detect single molecules [12–15]. These nanoparticle biosensors have nanoscale

---

✉ Muhammad Anisuzzaman Talukder  
anis@eee.buet.ac.bd

Zunaid Omair  
zomair@eecs.berkeley.edu

<sup>1</sup> Department of Electrical Engineering and Computer Science, University of California, Berkeley, CA 94705, USA

<sup>2</sup> Department of Electrical and Electronic Engineering, Bangladesh University of Engineering and Technology, Dhaka, 1205, Bangladesh

<sup>3</sup> School of Electronic and Electrical Engineering, University of Leeds, Leeds, LS2 9JT, UK

dimensions and a sensitivity in the range of nanometer—at least an order of three greater than that of photonic and photonic–plasmonic hybrid cavity biosensors.

When electromagnetic waves are incident on metal nanoparticles that are much smaller than the incident wavelength, the collective oscillations of bound electrons create LSPR. The nanoparticle-based biosensors that use LSPR for detection of biomolecules are much more amenable to miniaturization and multiplexing than those commercially available surface plasmon polariton (SPP)-based biosensors [16, 17]. Therefore, metal nanoparticle-based biosensors are an ideal candidate for lab-on-a-chip or point-of-care diagnostic tools. The nanoparticles offer excellent and stable tunability of LSPR wavelength ( $\lambda_{\text{LSPR}}$ ) by varying their shape, size, and composition [18, 19]. Since the decay length of electromagnetic field is 40–50 times shorter in LSPR biosensors than in SPP biosensors [20, 21], nanoparticles can offer a much smaller sensing volume, and hence, become more suitable for single molecule detection.

Among the currently studied metal nanoparticles, gold nanorods (GNRs) have shown the highest promise in maximum field enhancement at the tips along with a mass-producible fabrication method [13]. It is possible to detect single molecules by selectively attaching the target molecules to the tip of a GNR and measuring the shift in LSPR spectra. GNR biosensors are sensitive, molecule-specific, easy to make, and capable of multiplexing for monitoring multiple molecular interactions simultaneously [22]. In addition to experimental demonstrations, GNR biosensors have been investigated theoretically to understand the excitation of localized surface plasmons [13]. However, plasmonic resonances are affected by the sensing environment and binding dynamics of biomolecules, and an in-depth analysis for GNR biosensors is still lacking. Therefore, it is important to investigate the effects on the sensitivity when the sensing environment and molecular

binding dynamics change. It is also important to understand whether such a biosensor is suitable for different critical pathogens.

In this work, we investigate the effects of the sensing environment, i.e., buffer, substrate, and ligands on the sensitivity of GNR biosensors. We calculate the detection volume for single molecules. We find that the detection volume is ideal for single molecule detection—large enough for many protein molecules but small enough to suppress the background noise. We investigate the kinetics and binding-position-specific sensitivity of GNR biosensors. We propose and show that a cladding layer on the GNR can increase the sensitivity by selectively attaching biomolecules to the tips where plasmonic field enhancement is maximum. We calculate the sensitivity of the GNR biosensor with a cladding layer for several critical pathogens such as thyroid cancer marker thyroglobulin and HIV marker glycoprotein. We find that the sensitivity of GNR biosensors is orders of magnitude greater than other label-free optical single molecule detection techniques.

## GNR Sensing System

A schematic illustration of a GNR biosensor is given in Fig. 1a. GNRs can be manufactured by a seed-mediated growth technique and then spin-coated onto a substrate of choice [23]. Before the nanorods are used for sensing, they are functionalized with ligands to attach target molecules to them. An appropriate choice of ligands depends on the target molecule. For example, if the target molecule is avidin-class of protein such as streptavidin or streptavidin-R-phycoerythrin, GNRs are functionalized with biotin [24]. To functionalize, first, GNRs are incubated in a solution of thiolated biotin for 1 h, and then, the biotin solution is flushed with phosphate-buffered saline (PBS),

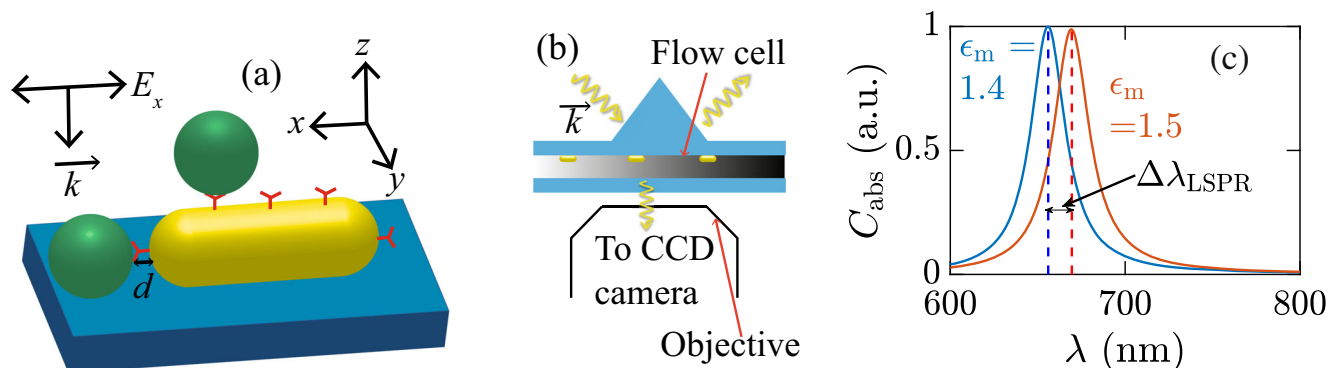


**Fig. 1** **a** Schematic illustration of a GNR biosensor. GNRs are functionalized with ligands and the target biomolecules are attached to the ligands. **b** Schematic illustration of a feasible experimental setup for the incidence of light and the detection of LSPR spectra. GNRs are

placed inside a flow cell through which the sample solution flows. **c** Absorption spectra without (blue) and with (red) a target molecule attached to the GNR. The difference between the frequencies of peak absorption of the two spectra is the shift in LSPR ( $\Delta\lambda_{\text{LSPR}}$ )

which results in a  $\sim 0.5$ -nm-thick biotin spacer layer around GNRs [13].

The choice of target molecules and ligand conjugates determines the ambient environment, i.e., buffer. An appropriate buffer is critical since even a small change in pH level can completely change most biological processes. An appropriate buffer is also crucial for the chemical stability of the target molecules, ligands, and GNRs [25]. In practice, the choice of suitable buffers in a GNR biosensor is limited to a few such as adenosine deaminase (ADA), 3-(*N*-morpholino) propanesulfonic acid (MOPS), phosphate buffer saline (PBS), 2-[tris(hydroxymethyl)-methyl-amino]-ethanesulfonic acid (TES), and piperazine-*N,N*-bis (2-hydroxypropanesulfonic acid) (POPSO), which have a pH in the range of 6.5–7.5. These buffers show sufficient inertness so that the target molecules, ligands, and GNRs remain chemically stable [26]. The substrate in the sensing system is a chemically inert dielectric medium. In this work, we use silicon dioxide ( $\text{SiO}_2$ ) as the substrate with a refractive index of 1.45, unless otherwise stated.

A feasible setup for the incidence of light and the detection of absorption spectrum in the GNR biosensor is schematically shown in Fig. 1b, which is similar to that presented in Ref. [22]. A fiber-coupled white-light-source or a superluminescent diode illuminates the prism. The prism helps the incident light fall normally on the GNR. The image of the flow cell is captured by a charge-coupled device (CCD) camera both before and after the excitation by the incident light. The LSPR spectrum of the GNR is determined from the difference of the spectral profiles of the two images. It is possible to detect a spectral resolution of 0.3 nm using this technique while taking shot noise into account [22]. The presence or absence of a target molecule can be detected from a measure of the shift of LSPR spectra ( $\Delta\lambda_{\text{LSPR}}$ ) when the target molecule attaches to or detaches from the GNR as shown in Fig. 1c.

## GNR Sensing Theory

When an electromagnetic wave is incident on a GNR, the conduction band electrons are set into oscillations, resulting in absorption and scattering of the incident field. The strength of oscillations is determined by the polarizability of the GNR. Gans [27] extended the Mie theory [28] to derive an analytical formulation for LSPR excitation of a prolate spheroid. GNRs can be approximated as prolate spheroids as shown in Fig. 1a, and the polarizability per unit volume can be written as [29, 30]:

$$\alpha(\omega) = \frac{\epsilon(\omega) - \epsilon_m(\omega)}{L\epsilon(\omega) + (1 - L)\epsilon_m(\omega)}, \quad (1)$$

where  $\epsilon$  and  $\epsilon_m$  are the dielectric permittivities of surrounding environment and gold metal, respectively, and  $L$  is the geometric factor given by:

$$L = \frac{1 - f^2}{f^2} \left[ \frac{1}{2f} \log_e \left( \frac{1 + f}{1 - f} \right) - 1 \right]. \quad (2)$$

In Eq. (2),  $f$  depends on the tip-to-tip distance  $a$  and diameter  $b$  of the GNR as  $f = \sqrt{1 - (b/a)^2}$ . Then, the absorption cross-section,  $C_{\text{abs}}$ , of GNRs can be calculated by [30]:

$$C_{\text{abs}} = k \text{Im}(\alpha), \quad (3)$$

where  $\text{Im}(\alpha)$  denotes the imaginary part of polarizability and  $k = 2\pi/\lambda$  is the wavevector, where  $\lambda$  is the wavelength of the incident light. Although GNRs absorb as well as scatter the incident electromagnetic waves, for small nanoparticles with feature sizes  $\ll \lambda$ , the absorption is much greater than the scattering [31, 32]. For GNRs with dimensions  $a = 31$  nm and  $b = 9$  nm that are considered in this work,  $C_{\text{abs}} \gtrsim 200C_{\text{scat}}$ , where  $C_{\text{scat}}$  is the scattering cross-section [33]. Hence, only  $C_{\text{abs}}$  can be assumed to be the signature of the interactions of the incident light with GNRs.

We note that Eq. (1) is valid when the  $x$ -component of the incident electric field is non-zero, i.e.,  $E_x \neq 0$ , which excites longitudinal LSPR in GNRs. By contrast, when the  $y$ -component of the incident electric field is non-zero, i.e.,  $E_y \neq 0$ , transverse LSPR is excited, which is not as sensitive as longitudinal LSPR. Additionally, transverse LSPR occurs at  $\sim 500$  nm, where the absorptions in both biological target samples and GNRs are significantly high. Therefore, transverse LSPR is usually considered unsuitable for biomolecule detection [34]. Moreover, the confined field is relatively uniformly distributed everywhere over the surface of the GNR for transverse LSPR, so that the field intensity at any point is much smaller than that at the tip of the GNR for longitudinal LSPR. Therefore, a GNR biosensor employing longitudinal LSPR is more sensitive to the change in  $\epsilon$  than that employing transverse LSPR.

In Eq. (1),  $\epsilon$  is the effective permittivity of the surrounding environment of a GNR that depends on the individual size, shape, and refractive indices of substrate, buffer, ligand, and target molecules. Therefore,  $\epsilon$  is not a simple mathematical average of refractive indices of substrate, buffer, ligand, and target molecules. Any change in the material or geometry of the surrounding components will change  $\epsilon$ , and hence,  $\lambda_{\text{LSPR}}$ . Therefore, when a target molecule is attached to the GNR,  $\epsilon$  of the environment changes, and hence,  $\lambda_{\text{LSPR}}$  changes. The change of  $\epsilon$  also depends on the location of the biomolecule where it is attached to the GNR. Therefore, to determine the sensitivity  $\Delta\lambda_{\text{LSPR}}$  in varying conditions, a numerical approach is

necessary that can include the size, shape, and refractive indices of the surrounding components.

## Simulation Methodology

To calculate the LSPR spectra of biosensors with and without biomolecules attached to them, we solve full-vectorial Maxwell's equations in three-dimensional space using the finite difference time domain (FDTD) method. We consider a broadband plane-wave light incident on the biosensor with wavelengths 600–1200 nm. Since both GNRs and biomolecules strongly absorb light at wavelengths  $\lesssim 600$  nm [35], we do not consider light with wavelengths  $< 600$  nm. In FDTD simulations, materials are modeled by their frequency-dependent complex refractive indices. Although Au is dispersive in the wavelength range of the incident light, dielectric materials including biomolecules are non-dispersive and non-absorbing [13]. Therefore, we consider biomolecules as dielectric materials with constant real refractive indices. The refractive indices of different biomolecules simulated in this work are given in Table 1. We use refractive indices of SiO<sub>2</sub> and Au from Palik [36], and Johnson and Christy [37], respectively.

The nanoscale dimensions of GNRs and biomolecules demand for ultra-fine mesh grids in FDTD simulations. We use rectangular mesh grids with a fixed size of 0.5 nm for a simulation region of  $100 \times 100 \times 100$  nm<sup>3</sup> that encompasses the biosensor system including the biomolecule. We have simulated with even smaller grid sizes and found no changes in the results. We use a perfectly matched layer (PML) boundary condition with 12 layers in the *x*- and *z*-directions. We find that if a greater number of PMLs is used at the boundaries, results do not change noticeably. However, if a smaller number of layers is used, simulations may diverge. Since the biosensor is symmetric in the *y*-direction as shown in Fig. 1a, we use a symmetric boundary condition in the *y*-direction, thus reducing the computation time by half.

In this work, we calculate  $C_{\text{abs}}$  within a region of  $90 \times 60 \times 40$  nm<sup>3</sup> that encompasses the GNR and the attached molecule. We calculate  $C_{\text{abs}}$  from the power absorbed per unit volume ( $P_{\text{abs}}$ ), which is calculated by

taking the divergence of the Poynting vector  $\vec{P}$  obtained from FDTD simulations as [38]:

$$P_{\text{abs}} = -0.5 \operatorname{Re}(\vec{\nabla} \cdot \vec{P}). \quad (4)$$

For a plane incident field, Eq. (4) can be written as:

$$P_{\text{abs}} = 0.5 \operatorname{Re}(i\omega \vec{E} \cdot \vec{D}^*), \quad (5)$$

where  $\vec{E}$  is the electric field,  $\vec{D}$  is the displacement vector, and  $\omega$  is the angular frequency. Now,  $C_{\text{abs}}$  is calculated by calculating the ratio of  $P_{\text{abs}}$  to the incident intensity  $I$  so that  $C_{\text{abs}} = P_{\text{abs}}/I$  [38].

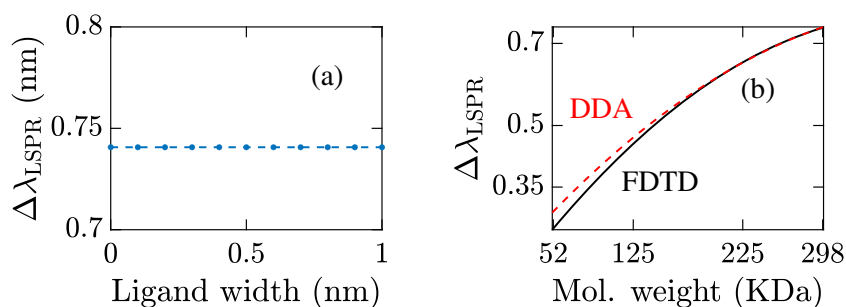
We consider only spherical shapes for biomolecules. Although biomolecule shapes may vary, a spherical shape produces the least shift in  $\lambda_{\text{LSPR}}$  when biomolecules are attached to GNRs [13]. Therefore, calculating the performance of a GNR biosensor for a spherical molecule is the measure of the performance for the worst-case scenario for molecules with same masses but different shapes. We also consider that the ligands are cylindrically shaped with a diameter of  $\sim 0.5$  nm and a height of  $\sim 0.5$  nm [13]. The small size of ligands does not affect the effective index of the medium, and hence, does not affect the LSPR spectra when the ligand size changes. We varied the diameter of biotin ligands while calculating the LSPR spectra for streptavidin-R-phycoerythrin molecules. We observed that  $\lambda_{\text{LSPR}}$  remains the same when biotin diameter is varied from 0 to 1 nm as shown in Fig. 2a.

To validate the developed FDTD model, we calculate  $\Delta\lambda_{\text{LSPR}}$  when a streptavidin-R-phycoerythrin protein molecule of variable weight is attached to one of the tips of the GNR using the developed model and compare to that reported in Ref. [13] using DDA simulations. We show the calculated  $\Delta\lambda_{\text{LSPR}}$  in Fig. 2b. We note that  $\Delta\lambda_{\text{LSPR}}$  values obtained from FDTD simulations closely match with those obtained from DDA simulations. There is a slight discrepancy in results when the weight of attached biomolecule is  $\lesssim 125$  kDa. However, the discrepancy in results can be neglected as the difference is  $\ll 0.3$  nm, which is the minimum spectral resolution that can be detected. The difference in results using FDTD and DDA techniques

**Table 1** Radius and refractive index of biomolecules considered in this work. Also, ligands necessary to attach the biomolecules to the GNR and calculated  $\Delta\lambda_{\text{LSPR}}$  due to the presence of biomolecules

Biomolecule	Radius (nm)	Refractive index	Ligand	$\Delta\lambda_{\text{LSPR}}$ (nm)
Streptavidin-R-phycoerythrin	4.5	1.45	Biotin	1.14
Thyroglobulin	4.84	1.45	Binding immunoglobulin protein	1.28
Glycoprotein 120	3.42	1.56	CD4	0.42

**Fig. 2** **a**  $\Delta\lambda_{\text{LSPR}}$  with diameter of biotin ligand in the detection of a streptavidin-R-phycoerythrin molecule. **b**  $\Delta\lambda_{\text{LSPR}}$  with molecular weight of biomolecule using FDTD and DDA simulations. DDA simulation results are taken from Ref. [13]



can be attributed to the differences of inherent numerical approaches adopted by the techniques [39].

## Results

### Longitudinal and Transverse LSPRs

In Fig. 3, we show electric field profiles due to the interactions of the incident light with a GNR biosensor without the target biomolecule. The electric field profiles are obtained using FDTD simulations. The incident light has electric field components  $E_x \neq 0$  and  $E_y \neq 0$  in Fig. 3a and b, respectively. We observe excitation of longitudinal LSPR and strong confinement of the incident light around the tips in Fig. 3a. By contrast, we observe excitation of transverse LSPR and confinement of the incident light along the entire surface of the GNR in Fig. 3b. The peak electric field in longitudinal LSPR is 26 times greater than that in transverse LSPR. Therefore, a GNR biosensor designed for longitudinal LSPR excitation with biomolecules attached to the tips will show much greater sensitivity than that designed for transverse LSPR excitation and/or with biomolecules attached to the body away from the tips.

### Effect of Environment on Sensitivity

#### Substrate

In this work, we have used  $\text{SiO}_2$  as the substrate, which is often used as the substrate in similar systems [13, 22].

However, the material and hence the refractive index of the substrate ( $n_s$ ) may vary. We have studied the effects of the substrate on the effective refractive index ( $n$ ) of the surrounding environment of a GNR biosensor. The results are presented in Fig. 4a. We note that the value of  $n$  is dominated by the value of  $n_s$  mainly due to the size of the substrate. Therefore,  $n$  can be tuned with the choice of the substrate. Ideally, a large difference between  $n$  and the refractive index of the target biomolecule is expected so that the sensitivity of detection is high. Therefore, it is important to understand the relation between  $n$  and  $n_s$  so that a highly sensitive GNR biosensor can be designed.

#### Buffer

The refractive indices of commonly used biological buffers ( $n_b$ ) are in the range of 1.30~1.37 [40]. However, there are few buffers that can have a much higher refractive index, e.g., POPSO has a refractive index of 1.593 [41]. Since buffer is the host medium for the target biomolecule, the sensitivity of a biosensor significantly depends on the contrast of the refractive indices of the buffer and the biomolecule. We varied the index of buffer from 1.3 to 1.6 and calculated  $\Delta\lambda_{\text{LSPR}}$  when a single streptavidin-R-phycoerythrin molecule is attached to one of the tips of a GNR. The change in  $\Delta\lambda_{\text{LSPR}}$  is given in Fig. 4b. We note that there is a change of sign of  $\Delta\lambda_{\text{LSPR}}$  from positive to negative when  $n_b > 1.45$ , which is the refractive index of the target molecule streptavidin-R-phycoerythrin. When a biomolecule attaches to the biosensor, it increases the effective index if it has a greater refractive index than that

**Fig. 3** Electric field profiles in **a** longitudinal LSPR excitation and **b** transverse LSPR excitation. The color bar has been normalized by the peak electric field in transverse LSPR excitation

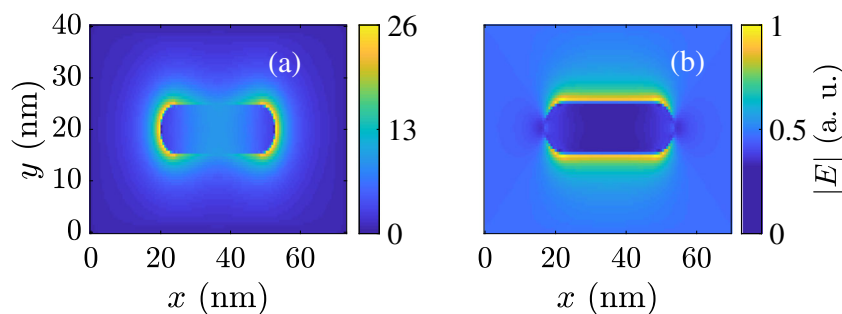
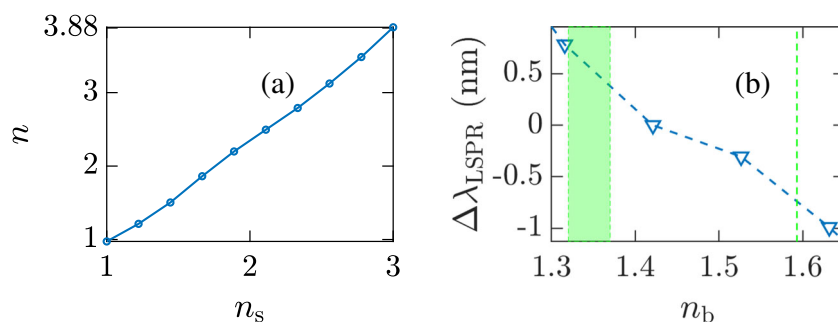


**Fig. 4** **a** Effective refractive index ( $n$ ) with the change of refractive index of substrate ( $n_s$ ). **b**  $\Delta\lambda_{\text{LSPR}}$  with the change of refractive index of the buffer medium ( $n_b$ ). The shaded region shows  $\Delta\lambda_{\text{LSPR}}$  for buffers ADA, MOPS, PBS, and TES. The green line shows  $\Delta\lambda_{\text{LSPR}}$  for buffer POPSO



of the buffer. By contrast, the effective index decreases if a biomolecule has a refractive index less than that of the buffer. Now, since  $\lambda_{\text{LSPR}}$  depends directly on the effective index of the biosensor [31], GNR biosensors can show either a red-shift or a blue-shift when biomolecules are attached depending on the difference of the refractive indices of the buffer and the target molecule. We also note that  $\Delta\lambda_{\text{LSPR}}$  increases as the difference between the indices of the buffer and the target molecule increases.

### Ligand

The choice of ligands depends on the surface chemistry of the target molecule and the biosensor. The ligands should attach the target molecule for a sufficiently long time for detection and should not affect the target molecule chemically. Hence, for a particular biosensor and target molecule, the choice of a ligand becomes specific. Table 1 shows a list of biomolecules and suitable ligands for those molecules. Now, the length of a ligand ( $d$ ) may vary over a range [13]. Since LSPR confines the incident light very close to the surface of the GNR, the sensitivity of a GNR biosensor would change due to the change in  $d$ . We have calculated the change in  $\lambda_{\text{LSPR}}$  when the length of biotin ligand varies in the detection of a streptavidin-R-phycoerythrin molecule. The results are presented in Fig. 5a. We note that  $\Delta\lambda_{\text{LSPR}}$  decreases exponentially as  $d$  increases. When  $d \gtrsim 3$  nm,  $\Delta\lambda_{\text{LSPR}}$  significantly decreases and the biosensor becomes insensitive

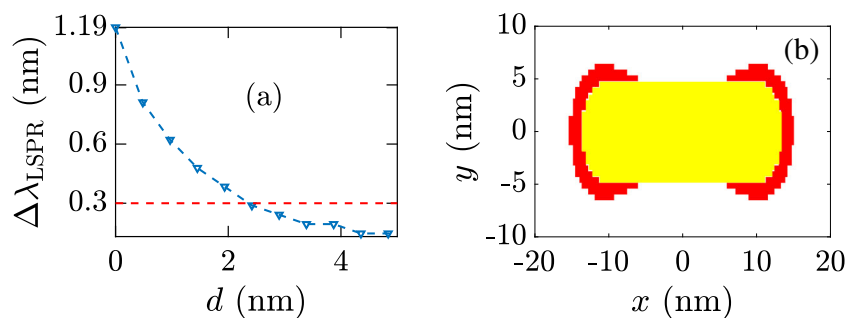
to the presence of a streptavidin-R-phycoerythrin molecule when  $d > 5$  nm.

Now, the decrease of  $\Delta\lambda_{\text{LSPR}}$  with the increase of ligand length defines the detection volume of a GNR biosensor. We calculate the detection volume for streptavidin-R-phycoerythrin molecules with biotin ligands. We assume  $\Delta\lambda_{\text{LSPR}} = 0.3$  nm as the sensitivity limit for detection. In Fig. 5a, we find that  $\Delta\lambda_{\text{LSPR}} \gtrsim 0.3$  nm when  $d \lesssim 2.4$  nm near the tip of the GNR. Proceeding similarly, we can calculate the detection volume around the GNR. We place molecules at different points on the surface of the GNR and find out  $d$  where  $\Delta\lambda_{\text{LSPR}}$  is 0.3 nm. By changing the position of the biomolecule over the GNR, we find a region where  $\Delta\lambda_{\text{LSPR}} \gtrsim 0.3$  nm, which is the detection volume. In Fig. 5b, we show the detection volume as a shaded region around the GNR. We numerically calculated the detection volume of the GNR as  $\sim 990$  nm<sup>3</sup>.

### Kinetics

Until now, we have presented the results for only one molecule attached to one of the tips of the GNR. In practice, in a finite detection time, several single molecular events are expected to occur. A tip-specific ligand functionalization of the GNR decreases the possibility of attaching the biomolecules to the body away from the tips. Nevertheless, it is possible that molecules attach to the body of the GNR [13]. An investigation of time-resolved kinetics of single molecule events and binding-position-specific sensitivity

**Fig. 5** **a**  $\Delta\lambda_{\text{LSPR}}$  due to the presence of a streptavidin-R-phycoerythrin molecule with the change in biotin ligand length ( $d$ ). **b** The red-shaded region around the GNR represents the region where the LSPR shift is  $\gtrsim 0.3$  nm for detection of streptavidin-R-phycoerythrin molecules with biotin ligands



in a GNR biosensor is important. For this investigation, we assume that the biomolecules attach one-by-one to the surface of the GNR in two different ways: (1) One of the molecules attaches to one of the tips first, and then other molecules attach to the body one by one as shown in Fig. 6a; (2) two of the molecules attach to the two tips first, and then other molecules attach to the body one by one as shown in Fig. 6b. We calculate  $C_{\text{abs}}$  and  $\lambda_{\text{LSPR}}$  from FDTD simulations when streptavidin-R-phycoerythrin molecules attach to the GNR according to the ways mentioned above. Using the calculated  $\lambda_{\text{LSPR}}$ , and Eqs. (1) and (3), we calculate the change in effective refractive index  $n$  of the surrounding environment when one or more molecules attach to the GNR.

The calculated  $\Delta\lambda_{\text{LSPR}}$  and  $n$  are shown in Fig. 6c and e, respectively, when biomolecules attach to the GNR according to the first scheme. The calculated changes in  $\Delta\lambda_{\text{LSPR}}$  and  $n$  are shown in Fig. 6d and f, respectively, when biomolecules attach to the GNR according to the second scheme. For both schemes, we note that  $\Delta\lambda_{\text{LSPR}} > 0.3$  nm when each molecule attaches to the GNR so that the single molecule events are easily detectable. We also note that the changes in  $\Delta\lambda_{\text{LSPR}}$  and  $n$  are sensitive to the position where the biomolecules attach to the GNR. The changes are greater when the biomolecules attach to the tips than that when they attach to the body away from the tips.

### Dielectric Cladding on GNR

To increase the sensitivity of a GNR biosensor, it is important to exploit the intense electric field confinement around tips. Therefore, to ensure that the biomolecules are attached to the tips, and hence, increase the sensitivity, we propose a cladding layer around the GNR that covers the body except the two tips. A schematic illustration of the proposed structure is shown in Fig. 7a. The electric field profile in the  $y = 0$  plane of a GNR biosensor with a dielectric cladding layer is shown in Fig. 7b. In the proposed structure, the target molecule will attach only to the tips of the GNR where the sensitivity is maximum. The proposed structure offers decreased ohmic losses incurred in the metal layer, and hence, an improved sensitivity in the detection of biomolecules. We calculate the  $\Delta\lambda_{\text{LSPR}}$  of a GNR biosensor with the cladding layer when a streptavidin-R-phycoerythrin molecule is attached to one of the tips. We assume that the cladding layer has a refractive index of 3.18 and a thickness of 3 nm. We note that several ternary and quaternary dielectric alloys have refractive indices close to 3.18. We find a  $\Delta\lambda_{\text{LSPR}}$  of 1.14 nm from a GNR with the cladding layer, which is an enhancement  $\sim 58\%$  from that of a GNR without the cladding layer.

GNR biosensors have shown a  $\Delta\lambda_{\text{LSPR}}$  sensitivity orders of magnitude greater than that obtained from photonic

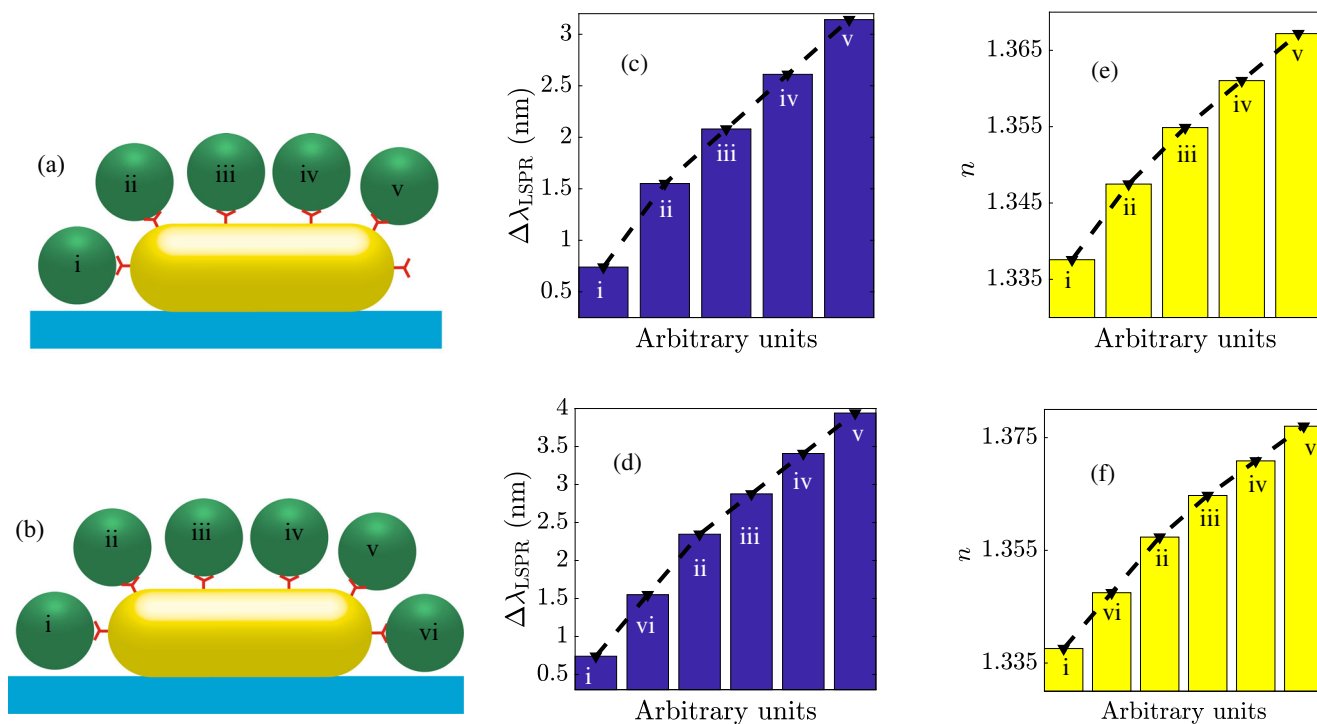
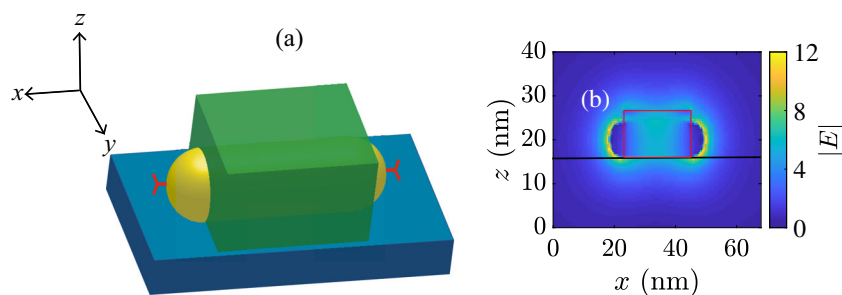


**Fig. 6** **a** Scheme 1: One molecule attaches to one of the tips of the GNR first, then other molecules attach to the body one by one. **b** Scheme 2: Two molecules attach to the two tips of the GNR first, then other molecules attach to the body one by one.  $\Delta\lambda_{\text{LSPR}}$  when single

molecule events occur in **c** scheme 1 and **d** scheme 2. Effective refractive index ( $n$ ) of the surrounding medium when single molecule events occur in **e** scheme 1 and **f** scheme 2

**Fig. 7** **a** Schematic illustration of a GNR with a cladding layer. **b** Electric field profile in the  $x$ - $z$  plane through  $y = 0$  of a GNR with a cladding layer



cavity-based biosensors [13]. We compared  $\Delta\lambda_{\text{LSPR}}$  that we obtained with a GNR biosensor with the cladding layer to that obtained using a photonic crystal nanobeam cavity platform reported in Ref. [11]. Using the same biological setup, we found an enhancement of  $\Delta\lambda_{\text{LSPR}}$  on the order of 4. We also calculated  $\Delta\lambda_{\text{LSPR}}$  for a yeast ribosome to compare the result to that reported using microtoroid optical resonators in Ref. [42]. We found a  $\Delta\lambda_{\text{LSPR}} \approx 1.71$  nm for a yeast ribosome when attached to a GNR with cladding layer, which is six orders of magnitude greater than that obtained using microtoroid optical resonators.

### Critical Pathogen Detection

We have extensively studied the sensitivity of a GNR biosensor while detecting streptavidin-R-phycoerythrin molecules. Here, we present the sensitivity of a GNR biosensor for detecting critical pathogens such as thyroglobulin and glycoprotein. Thyroglobulin molecule is a marker for thyroid cancer [43] and glycoprotein 120 molecule is a critical component to detect the existence of HIV [44]. Thyroglobulin molecule can be assumed spherical with a radius of 4.84 nm and a refractive index of 1.45 [43]. Glycoprotein 120 molecule can be assumed spherical with a radius of 3.42 nm and a refractive index of 1.56 [44, 45]. While thyroglobulin molecules conjugate with binding immunoglobulin protein, glycoprotein 120 molecules conjugate with CD4. Due to its inertness, PBS can be used as the buffer in the detection of both the pathogens. We find a  $\Delta\lambda_{\text{LSPR}}$  of 1.28 nm when thyroglobulin molecules are attached to the tips of a GNR with the cladding layer. We note that a  $\Delta\lambda_{\text{LSPR}}$  of only 17 fm has been observed using a biosensor based on a nanoplasmonic–photonic hybrid microcavity [43]. We find a  $\Delta\lambda_{\text{LSPR}}$  of 0.42 nm when glycoprotein 120 molecules are attached to the tips of a GNR with the cladding layer. We note that the  $\Delta\lambda_{\text{LSPR}}$  values for glycoprotein 120 are also orders of magnitude greater than that usually obtained for biomolecules in most photonic and photonic-plasmonic hybrid cavity biosensors. Therefore, GNR biosensors have the potential of successfully detecting single molecules of these critical pathogens, and hence, they are a promising candidate for early detection of many critical diseases. We summarize the results in Table 1.

### Conclusion

We have presented a comprehensive theoretical analysis of the sensitivity of GNR biosensors when the surrounding environment, i.e., substrate, buffer, and ligand, changes. We have found that the sensitivity critically depends on the substrate and buffer. The sensitivity does not depend on the diameter of ligands; however, it critically depends on the length of ligands as it determines the distance of the biomolecule from the GNR. The presented biosensor has a detection volume of  $\sim 990$  nm<sup>3</sup>, which is suitable for single molecule detection of many proteins that have a radius of  $\sim 5$ –10 nm. Single molecules can be attached to any position on the biosensor—on the tip or the on the body—and still be detected with sufficient sensitivity. Our proposed GNR biosensor with a dielectric cladding layer can increase the sensitivity further for detection of single molecules and detect the thyroid cancer marker thyroglobulin and HIV marker glycoprotein with orders of magnitude greater sensitivity than that obtained using other optical label-free biosensors.

### References

- Chowell D, Castillo-Chavez C, Krishna S, Qiu X, Anderson K (2015) Modelling the effect of early detection of Ebola. *Lancet Infect Dis* 15:148–149
- Powers K, Ghani A, Miller W, Hoffman I, Pettifor A, Kamanga G, Martinson F, Cohen M (2011) The role of acute and early HIV infection in the spread of HIV and implications for transmission prevention strategies in Lilongwe, Malawi: a modelling study. *Lancet* 378:256–268
- Saving lives and averting costs? The case for earlier diagnosis just got stronger, ([scienceblog.cancerresearchuk.org](http://scienceblog.cancerresearchuk.org), 2017), <http://scienceblog.cancerresearchuk.org/2014/09/22/saving-lives-and-averting-costs-the-case-for-earlier-diagnosis-just-got-stronger/>
- Single Molecule Detection, (Andor, 2016), <http://www.andor.com/learning-academy/single-molecule-detection-introduction>
- Kall M (2012) Biosensors: one molecule at a time. *Nat Nano* 7:347–349
- Bergveld P (1970) Development of an ion-sensitive solid-state device for neuro-physical measurements. *IEEE Trans Biomed Eng* 17:70–71
- Rocha-Santos TAP (2014) Sensors and biosensors based on magnetic nanoparticles. *Trends Anal Chem* 62:28–36
- Armani AM, Kulkarni RP, Fraser SE, Flagann RC, Vahala KJ (2007) Label-free, single-molecule detection with optical microcavities. *Science* 317:783–787

9. Arnold S, Shopova SI, Holler S (2009) Whispering gallery mode bio-sensor for label-free detection of single molecules: thermo-optic vs. reactive mechanism. *Opt Express* 18:281–287
10. Dentham VR, Holler S, Barbre C, Keng D, Kolchenko V, Arnold S (2013) Label-free detection of single protein using a nanoplasmonic-photonic hybrid microcavity. *Nano Lett* 13:3347–3351
11. Quan Q, Floyd DL, Burgess IB, Deotare PB, Frank IW, Tang SKY, Ilic R, Loncar M (2013) Single particle detection in CMOS compatible photonic crystal nanobeam cavities. *Opt Express* 21:32225–32233
12. Mayer KM, Hao F, Lee S, Nordlander P, Hafner JH (2010) A single molecule immunoassay by localized surface plasmon resonance. *Nanotechnology* 21:255503
13. Zijlstra P, Paulo PMR, Orrit M (2012) Optical detection of single non-absorbing molecules using the surface plasmon resonance of a gold nanorod. *Nat Nano* 7:379–382
14. Ament I, Prasad J, Hankel A, Schmachtel S, Sönnichsen C (2012) Single unlabeled protein detection on individual plasmonic nanoparticles. *Nat Nano* 12:1092–1095
15. Stockman MI (2015) Nanoplasmonic sensing and detection. *Science* 348:287–288
16. Hill RT (2015) Plasmonic biosensors. *Wiley Interdiscip. Rev Nanomed Nanobiotechnol* 7:152–168
17. Biacore life sciences, (GE Healthcare, 2016), <https://www.biacore.com/lifesciences/in-dex.html>
18. Mock JJ, Barbic M, Smith DR, Schultz DA, Schultz S (2002) Shape effects in plasmon resonance of individual colloidal silver nanoparticles. *J Chem Phys* 116:6755–6759
19. Anker JN, Hall WP, Lyandres O, Shah NC, Zhao J, Duyne RPV (2008) Biosensing with plasmonic nanosensors. *Nat Mat* 7:442–453
20. Whitney AV, Elam JW, Zou S, Zinovev AV, Stair PC, Schatz GC, Duyne RPV (2005) Localized surface plasmon resonance nanosensor: a high-resolution distance-dependence study using atomic layer deposition. *J Phys Chem B* 109:20522–20528
21. Haes AJ, Zou S, Schatz GC, Duyne RPV (2003) A nanoscale optical biosensor: the long range distance dependence of the localized surface plasmon resonance of noble metal nanoparticles. *J Phys Chem B* 108:109–116
22. Beuwer MA, Prins MWJ, Zijlstra P (2015) Stochastic protein interactions monitored by hundreds of single-molecule plasmonic biosensors. *Nano Lett* 15:3507–3511
23. Nikoobakht B, El-Sayed MA (2003) Preparation and growth mechanism of gold nanorods (NRs) using seed-mediated growth method. *Chem Matter* 15:1957–1962
24. Bayer EA, Wilcheck M (2009) The use of avidin-biotin complex as a tool in molecular biology. In: Glick D (ed) *Methods of Biochemical Analysis*. Wiley, Hoboken
25. Requirements for biological buffers, (Applichem, 2017), <https://www.applichem.com/en/products/laboratory-biochemicals/biological-buffer/>
26. BioBuffer (2019) <https://www.applichem.com/fileadmin/Broschueren/BioBuffer.pdf>
27. Gans R (1912) Über die Form ultramikroskopischer Goldteilchen. *Ann Phys* 342:881–900
28. Mie G (1908) Beiträge zur optik trüber medien, speziell kolloidaler metallösungen. *Ann Phys* 330:377–445
29. Rysselberghe PV (1932) Remarks concerning the Clausius-Mossotti law. *J Phys Chem* 36:1152–1155
30. Bohren CF, Huffman DR (2007) Absorption and Scattering of Light by Small Particles. Wiley Online Library, Chap. 5
31. Maier CA (2007) *Plasmonics: Fundamentals and Applications*. Springer, USA. Chap. 5
32. Koya AN, Ji B, Hao Z, Lin J (2015) Resonance hybridization and near field properties of plasmonic ring dimer-rod nanosystem. *J Appl Phys* 118:113101
33. Mackey MA, Ali MRK, Austin LA, Near RD, El-Sayed MA (2014) The most effective gold nanorod size for plasmonic photothermal therapy: theory and in vitro experiments. *J Phys Chem B* 118:1319–1326
34. Huang X, Neretina S, El-Sayed MA (2009) Gold nanorods: from synthesis and properties to biological and biomedical applications. *Adv Mater* 21:4880–4910
35. Nilsson PO, Norris C, Wallden L (1969) Evidence for direct transitions from the d-band of gold. *Solid State Commun* 7:1705–1707
36. Palik ED (1993) *Handbook of Optical Constants of Solids*. Elsevier
37. Johnson PB, Christy RW (1972) Optical constants of the noble metals. *Phys Rev B* 6:4370–4379
38. Absorption per unit volume, (Lumerical knowledge base, 2016), [https://kb.lumerical.com/en/layout\\_analysis\\_pabs.html](https://kb.lumerical.com/en/layout_analysis_pabs.html)
39. Kahnert FM (2003) Numerical methods in electromagnetic scattering theory. *J Quant Spectros Radia Transfer* 79–80:775–824
40. Dieguez L, Mir M, Martinez E, Moreno M, Samitier J (2009) Effect of the refractive index of buffer solutions in evanescent optical biosensors. *Sens Lett* 7:851–855
41. POPSO, (CAS database, 2017), <http://www.chembk.com/en/cas>
42. Su J, Goldberg AF, Stoltz BM (2016) Label-free detection of single nanoparticles and biological molecules using microtoroid optical resonators. *Light Sci Appl* 5:e16001
43. Dantham VR, Holler S, Barbre C, Keng D, Kolchenko V, Arnold S (2013) Label-free detection of single protein using a nanoplasmonic-photonic hybrid microcavity. *Nano Lett* 13:3347–3351
44. Cullen DC, Brown RGW, Lowe CR (1987) Detection of immuno-complex formation via surface plasmon resonance on gold-coated diffraction gratings. *Biosensors* 3:211–225
45. Envelope glycoprotein GP120, (Wikipedia, 2016), [https://en.wikipedia.org/wiki/Envelope\\_glycoprotein\\_GP120](https://en.wikipedia.org/wiki/Envelope_glycoprotein_GP120)

**Publisher's Note** Springer Nature remains neutral with regard to jurisdictional claims in published maps and institutional affiliations.